

## Article

# Mechanical and Tribological Behavior of Gravity and Squeeze Cast Novel Al-Si Alloy

Vadlamudi Srinivasa Chandra<sup>1,2</sup>, Koorella S. V. B. R. Krishna<sup>2</sup>, Manickam Ravi<sup>3</sup>, Katakam Sivaprasad<sup>1,\*</sup>, Subramaniam Dhanasekaran<sup>2</sup> and Konda Gokuldoss Prashanth<sup>4,5,6,\*</sup>

<sup>1</sup> Advanced Materials Processing Laboratory, Department of Metallurgical and Materials Engineering, National Institute of Technology, Tiruchirapalli 620015, India; Srinivasachandra.V@ashokleyland.com

<sup>2</sup> Ashok Leyland Limited, Technical Center, Chennai 600103, India; Koorella.krishna@ashokleyland.com (K.S.V.B.R.K.); s.dhanasekaran@ashokleyland.com (S.D.)

<sup>3</sup> National Institute for Interdisciplinary Science and Technology, Thiruvananthapuram 695019, India; ravi@niist.res.in

<sup>4</sup> Department of Mechanical and Industrial Engineering, Tallinn University of Technology, Ehitajate Tee 5, 19086 Tallinn, Estonia

<sup>5</sup> Erich Schmid Institute of Materials Science, Austrian Academy of Sciences, Jahnstrasse 12, 8700 Leoben, Austria

<sup>6</sup> Center for Biomaterials, Cellular, and Molecular Theranostics, Vellore Institute of Technology, Vellore 632014, India

\* Correspondence: ksp@nitt.edu (K.S.); kgprashanth@gmail.com (K.G.P.)

**Abstract:** The automotive industry traditionally reduces weight primarily by value engineering and thickness optimization. However, both of these strategies have reached their limits. A 6% reduction in automotive truck mass results in a 13% improvement in freight mass. Aluminum alloys have lower weight, relatively high specific strength, and good corrosion resistance. Therefore, the present manuscript involves manufacturing Al-based alloy by squeeze casting. The effect of applied pressure during the squeeze cast and gravity cast of a novel Al-Si alloy on microstructural evolution, and mechanical and wear behavior was investigated. The results demonstrated that squeeze casting of the novel Al-Si alloy at high-pressure exhibits superior mechanical properties and enhanced wear resistance in comparison to the gravity die-cast (GDC) counterpart. Squeeze casting of this alloy, at high pressure, yields fine dendrites and reduced dendritic arm spacing, resulting in grain refinement. The finer dendrites and reduced dendritic arm spacing in high-pressure squeeze cast alloy than in the GDC alloy were due to enhanced cooling rates observed during the solidification process, as well as the applied squeeze pressure breaks the initial dendrites that started growing during the solidification process. Reduced casting defects in the high-pressure squeeze cast alloy led to a reduced coefficient of friction, resulting in improved wear resistance even at higher loads and higher operating temperatures. Our results demonstrated that squeeze casting of the novel Al-Si alloy at high-pressure exhibits a 47% increase in tensile strength, 33% increase in hardness, 10% reduction in coefficient of friction, and 15% reduction in wear loss compared to the GDC counterpart.

**Keywords:** squeeze casting; novel Al-Si alloy; wear analysis; microstructure; mechanical properties; pin on disc wear testing



**Citation:** Chandra, V.S.; Krishna, K.S.V.B.R.; Ravi, M.; Sivaprasad, K.; Dhanasekaran, S.; Prashanth, K.G. Mechanical and Tribological Behavior of Gravity and Squeeze Cast Novel Al-Si Alloy. *Metals* **2022**, *12*, 194. <https://doi.org/10.3390/met12020194>

Academic Editor: Wenming Jiang

Received: 3 January 2022

Accepted: 19 January 2022

Published: 21 January 2022

**Publisher's Note:** MDPI stays neutral with regard to jurisdictional claims in published maps and institutional affiliations.



**Copyright:** © 2022 by the authors. Licensee MDPI, Basel, Switzerland. This article is an open access article distributed under the terms and conditions of the Creative Commons Attribution (CC BY) license (<https://creativecommons.org/licenses/by/4.0/>).

## 1. Introduction

According to the International Energy Association report of 2019, the transportation industry is the second largest contributor to global CO<sub>2</sub> emissions (at 27%) [1]. The automotive industry globally is striving to reduce CO<sub>2</sub> emissions by light-weighting, improving the efficiency of internal combustion engines, usage of alternate fuels, etc. A 10% reduction in mass results in a 6% improvement in fuel efficiency, by which CO<sub>2</sub> emission will be reduced significantly over the lifetime of the vehicle [1].

Aluminum, being light in comparison to steel, is an excellent choice of material for weight reduction in automobile and aerospace sectors (where it is available in both sheet and cast forms) [2–5]. The aluminum industry offers a wide range of aluminum alloys with various combinations of strength, ductility, wear, and corrosion resistance [6–8]. Many elemental combinations are used to alloy with aluminum as solute [9,10]. Small quantities of elements such as silicon, manganese, iron, chromium, molybdenum, etc. are added in aluminum to enhance its mechanical and physical properties and to improve some of the specific properties required in strategic applications [11–13]. In almost all production industries and in day-to-day life, Al-Si cast alloys play a vital role due to their ease in castability, corrosion resistance, and high mechanical properties [14–16]. Al-Si alloys are widely used in various industries due to their excellent mechanical properties, improved wear and thermal behavior, supreme corrosion resistance, and excellent castability [8,17–19]. The addition of Cu and Fe to this alloy further enhances the mechanical and wear behavior of the material without heat treatment [20–22]. The addition of Copper imparts strength and hardness to the casting [20,22]. The properties achieved by the addition of Fe are comparable to those alloys with various heat-treated and aged Aluminum alloys. Optimized Fe alloying aids for the possibility to reduce the aging time without the addition of Mg, resulting in significant cost saving which is the need of the hour in any industry [23,24].

Iron tends to form intermetallic with other alloying elements resulting in strengthening of the alloy with enhanced wear and thermal behavior [24]. The intermetallics formed are usually hard and brittle with a superior high-temperature behavior. Thus, novelty in conventional Al-Si casting alloys, by the addition of Cu and Fe during the casting process, can result in enhanced performance of the cast product [20–23]. Further, the addition of Fe improves fluidity, a vital requirement to produce a sound casting. Taylor et al. suggested having a critical percentage of Fe based on the silicon percentage in the alloy. If Fe exceeds the critical percentage, it would influence loss of ductility due to shrinkage porosity [23,25]. Enhanced fluidity provides an opportunity for the production of thin-walled castings [26]. Intricate shapes with a near-net finish are possible due to the improved fluidity. 4XXX series wrought alloy has a UTS of ~134 MPa and YS of ~64 MPa and novel Al-Si alloy is expected to have the UTS of ~385 MPa and YS of ~240 MPa [18,19,27–29]. There is a significant enhancement of mechanical properties by the addition of an optimum percentage of Fe, without any thermal treatment leading to huge cost savings [24]. Hence, such novel Al-based alloys can be utilized in a variety of applications, due to their superior mechanical and thermal properties. In addition, it can find a prominent place in automotive industry, where light-weighting at a lower cost is a beneficial advantage. Some of the remarkable advantages of die-casting over conventional sand casting are an increase in productivity, dimensional accuracy of as-cast components, and better mechanical properties as a result of improved microstructural features [30].

Squeeze casting is both economical and has the potential to create cast components with minimal defects, often achieving near-net-shaped components [31–33]. In addition, die-casting reduces the metal wastages which arise due to the use of feeders and risers as in conventional sand casting [34]. Squeeze casting is a combination of the casting and forging processes where the solidification of molten metal takes place under pressure, thereby reducing the casting defects created due to gas entrapments as well as increasing the ductility of the resultant component. The squeeze casting process parameters play an important role in determining the microstructure of the cast components. The process parameters such as squeeze pressure, squeeze pressure duration, pouring temperature, and die temperatures have overall control on the microstructure [35]. The squeezing pressure increases the heat transfer rate in between the mold interfaces that enhance the surface finish and also help to create a uniform microstructure from surface to core [36]. For any new alloys or modified alloys, process parameters have to be optimized for better microstructure and mechanical properties [37]. In the squeeze casting process, the desirable mechanical and microstructure features are based on the combination of mold casting and die forging due to the fact that the molten metal is solidified under hydrostatic

pressure. This would have better control over mechanical properties as well as lead to a homogenous microstructure [38]. In addition, the squeeze-casting process creates a very fine microstructure and also eliminates the gas and shrinkage porosities [39]. Reports on the Fe-addition to Al-Si alloy show that for the Al-Si alloy with Fe, the mechanical properties depend not only on chemical composition but also on the microstructural morphology of the phases (such as the Al-rich alpha phase and eutectic Si phase) [40].

Since the addition of alloy elements to Al lead to the formation of coarse microstructure in the as-cast condition and to obtain finer microstructure suitable strategies need to be followed [41–45]. Fine microstructure can be the addition of grain refiners [44–46], severe plastic deformation [47,48], cryomilling [49], high pressure solidification [50,51], laser processing [52,53], etc. Accordingly, the present investigation aims to study utilize the low-cost fabrication technique (squeeze pressure casting) and explore the influence of applied squeeze pressure on the microstructure during the solidification of a molten Al-Si-Cu-Fe alloy. The influence of squeeze pressure on the mechanical and wear behavior of the alloy is investigated in detail.

## 2. Experimental Procedure

Samples considered in the present study are processed through gravity die casting (GDC), low-pressure squeeze casting (LPSC) at 5 MPa, and high-pressure squeeze cast (HPSC) at 12 MPa respectively using a cylindrical mold made up of H13 steel. The chemical composition of the alloy in various cast conditions are determined using an optical emission spark (OES) spectrometer and are listed in Table 1.

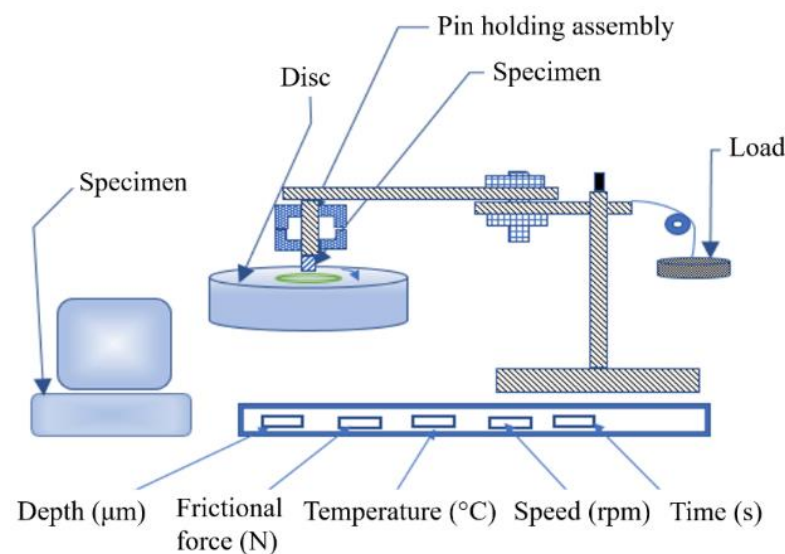
**Table 1.** Chemical composition of novel alloy designed.

| Element/Weight % | Al    | Si   | Cu   | Mg    | Fe    | Zn    | Mn   | Ni    | Cr    |
|------------------|-------|------|------|-------|-------|-------|------|-------|-------|
| GDC              | 91.02 | 5.41 | 2.97 | 0.373 | 0.135 | 0.019 | 0.01 | 0.005 | 0.001 |
| LPSC             | 91.09 | 5.41 | 2.91 | 0.372 | 0.135 | 0.016 | 0.01 | 0.006 | 0.001 |
| HPSC             | 90.99 | 5.41 | 2.98 | 0.391 | 0.142 | 0.017 | 0.01 | 0.005 | 0.001 |

Microstructural analysis of the samples (under various casting conditions) was observed using an optical microscope (LEICA DMLM, Mumbai, India; 50× to 1000× range). The hardness measurements were carried out using a Zwick Roell Vickers microhardness tester (from Zwick, Gurugram, India) at a test load of 0.1 kgf with a dwell time of 10 s. Tensile testing was performed using a Tinius Olsen H25KL tabletop tensile testing unit (from Tinius Olsen, Noida, India) with a strain rate of  $5 \times 10^{-4}$ /s as per ASTM-E08-2016 standard using a sub-sized specimen [54]. Wear testing was carried out using a pin on disc wear testing machine (Ducom, Bangalore, India) based on the ASTM G99-05 standard [55]. Wear tests were carried out with a sliding velocity set to 0.314 m/s and measured for the sliding distance of 1000 m [56–58]. The sliding disc diameter is 30 mm, the speed of the machine is held at 200 rpm and the test time is considered to be around 3185 s. The machine disc is made up of EN31 material with a roughness of 10 μm and hardness ~60 HRC. The wear testing was carried out with different test variables to understand the behavior of Al-Si alloys as a function of changing parameters. Three different loads were applied (20 N, 40 N, and 60 N) at a higher operating temperature of 200 °C, refer to Table 2. The schematic of the wear testing unit is illustrated in Figure 1. The wear testing machine consists of a specimen in the form of a pin and it is tested against a disc made of EN31 material according to the ASTM G99-05 standards. In addition, the load is applied through the loading panel, and the entire equipment is operated using a computer-based controller. All of the parameters including depth, force, temperature, speed of the disc, time, etc. can be controlled using the controller in an acute fashion. The surface morphological features of all of the tensile fractured samples and worn-out surfaces from wear tests were studied using an FEI Quanta 200 Scanning electron microscope (SEM) (FEI, Bangalore, India).

**Table 2.** Al-Si alloys wear test input parameters.

| Experiment Number | Casting Route | Applied Load (N) | Temperature (°C) |
|-------------------|---------------|------------------|------------------|
| 1-A1              | GDC           | 20               | 200              |
| 1-A2              | GDC           | 60               | 200              |
| 1-A3              | GDC           | 40               | 200              |
| 1-B1              | LPSC          | 20               | 200              |
| 1-B2              | LPSC          | 60               | 200              |
| 1-B3              | LPSC          | 40               | 200              |
| 1-C1              | HPSC          | 20               | 200              |
| 1-C2              | HPSC          | 60               | 200              |
| 1-C3              | HPSC          | 40               | 200              |

**Figure 1.** Schematic representation of the pin-on-disc wear testing unit.

### 3. Results and Discussion

#### 3.1. Microstructure

The microstructure of GDC, LPSC, and HPSC samples are shown in Figure 2 using optical (Figure 2a–c) and scanning electron microscopy (Figure 2d–f). The microstructure of the GDC specimen has coarse dendrites as shown in Figure 2a. The microstructure gets refined with the application of pressure. The LPSC and HPSC samples have shown the presence of small dendrites, which are also deformed. They are not in a continuous state like the GDC samples. An increase in the squeeze-pressure increases the cooling rate, resulting in higher nucleation and finer dendritic size with large dendrite spacing. Similar observations were made by Amar et al. [59], where the 2017A alloy was squeeze cast using GDC and at high pressures. Moreover, Amar et al. have shown that with the application of pressure, a refined and homogeneous microstructure was observed, which is in agreement with the present results. The heat inside the mold and pressure have a significant effect on the size of the dendrites, dendritic morphology, and the distribution of microstructural constituents. Increasing the squeeze casting pressure refined all microstructural features (including the size of the microstructural features and arm spacing of dendrites) and modified the morphology of Al-Si eutectic phases. Further, dendrites were small and almost spherical in shape in squeeze cast conditions. In GDC alloys, the dendrites were observed to have an elongated plate-like morphology (Figure 2d), whereas, in the other two alloys (Figure 2e,f), cast microstructures consist of needle-like morphologies. In all of the samples, the Al-Si-Fe regions are constrained within the inter-dendritic regions due to kinetic differences between the phases. These phases were formed as curved crystals and in some regions, it exhibits plate-like morphology joined along with irregular, curved surfaces.

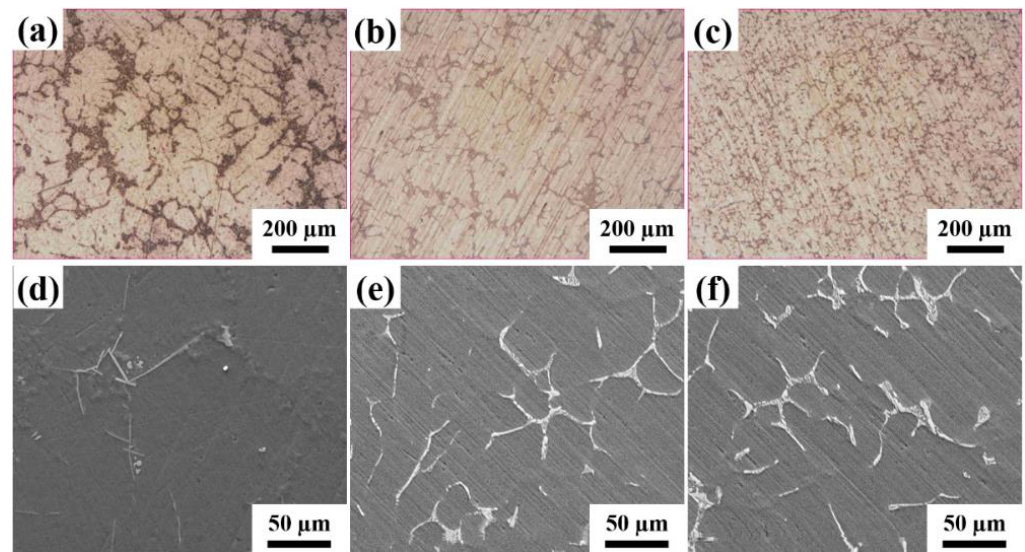


**Figure 2.** (a–c) Optical micrographs and (d–f) scanning electron microscopy images of the cast samples fabricated by (a,d) GDC route, (b,e) LPSC route, and (c,f) HPSC route, respectively.

### 3.2. Hardness

The hardness analysis was carried out to study the variation of hardness along the cast cross-section from the surface to the middle of the cast sample in all three-process conditions, *viz.*, GDC, LPSC, and HPSC, respectively. The results shown in Figure 3 indicate that the squeeze-cast sample with higher pressure exhibits a higher hardness. Lin et al. studies on the Al-based alloys showed a hardness of 75 HV and 85 HV for GDC and high-pressure squeeze cast materials [38]. Similarly, Thirumal et al. [39] studies on AA6061 alloy castings as a function of different squeeze-cast pressures show an increase in the hardness of the alloy with an increase in the pressure. The results from Lin et al. and Thirumal et al. are in agreement and are similar to the results from the present study. In addition, there is significant variation in hardness values as observed from the surface to core, indicating the absence of porosity and other casting defects.

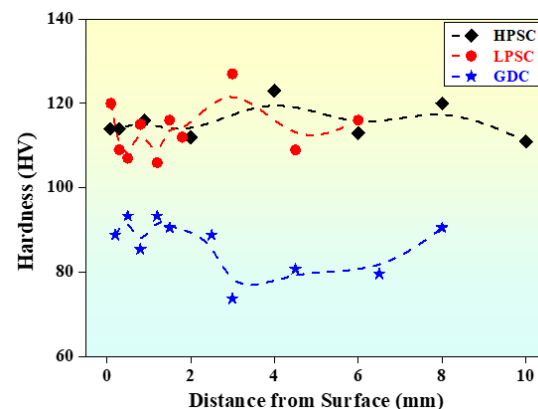


**Figure 3.** Microhardness survey taken for the cast samples in all three conditions (gravity die casting (GDC), low-pressure squeeze-casting (LPSC), and high-pressure squeeze-casting (HPSC) taken from surface to center of the casting).

The hardness observations from the surface to the core also indicate that the cast structure is homogenous and uniform. On the other hand, the LPSC sample shows similar hardness values to the high-pressure squeeze-cast sample along the surface. However, the hardness values show some fluctuations when measured from the surface to the core, unlike the high-pressure squeeze-cast samples. This corroborates the presence of defects

(such as porosity) in these LPSC samples. Similarly, the GDC sample shows inferior hardness when compared to the squeeze-case samples due to reduced cooling rates. In addition, the hardness fluctuates between 95 HV to 75 HV as we move from the surface to the core showing the presence of defects/imperfections in these samples. Based on the hardness survey and microstructural correlation, it is evident that squeeze pressure is one of the most significant process parameters for achieving higher material properties with uniform distribution in the squeeze-casting process. This is in good agreement with the discussion carried out by Azhagan et al. [39] and Mohamed et al. [59]. In addition, the hardness of the alloy increases with the application of pressure. This enhanced behavior in HPSC and LPSC alloys in comparison with GDC alloy was due to improvements in heat transfer rates during solidification due to the applied pressure, resulting in refinement of microstructure and the improved contact area between the die and molten metal surface [50,51,60,61].

### 3.3. Tensile Properties

Tensile properties of the investigated GDC and other two-squeeze cast samples are shown in Figure 4. The HPSC sample has shown a tensile strength of ~540 MPa against LPSC at ~382 MPa and GDC at ~367 MPa. On comparing GDC and squeeze cast alloys, the mechanical properties are superior for the LPSC and HPSC alloys. The results explain that the samples fabricated by the squeeze-casting process exhibit higher yield and tensile strength as compared to samples fabricated by the GDC process. In the squeeze-cast samples, the tensile and yield strength of the alloy increases with increasing pressure. A decrease in the grain size with an increase in squeeze casting pressure results in an increased grain boundaries volume. The increased grain boundary volume increases the resistance to dislocation movement, resulting in enhanced strength properties [62–64]. As pressure was held on molten metal during the squeeze casting process until the end of the solidification process, the rate of heat transfer was increased and macro and microporosity had been eliminated in comparison to the GDC process, resulting in enhanced mechanical properties. The elongation observed for the cast samples (GDC, to be almost similar with LPSC, and HPSC) is similar within the experimental conditions.

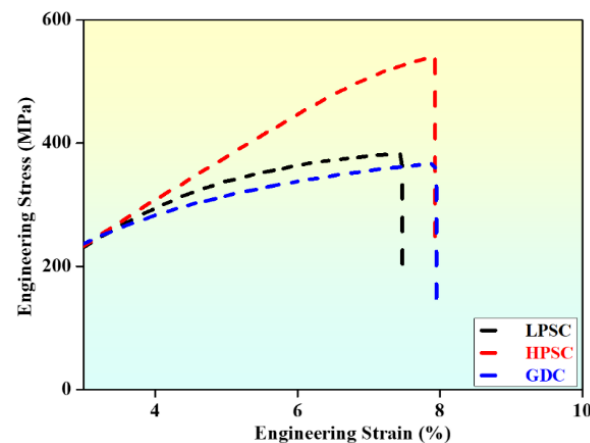


**Figure 4.** Engineering stress-strain curves of the cast samples fabricated under different conditions (gravity die-casting, low-pressure squeeze casting, and high-pressure squeeze casting).

### 3.4. Wear Behavior

The wear behavior of all three samples fabricated by the three casting routes (namely GDC, LPSC, and HPSC) were studied to understand their tribological behavior. The wear test results in terms of coefficient of friction (COF) and wear loss are shown in Figure 5. The COF increases with an increase in the working temperature. However, with the application of pressure at the same condition, the COF decreases in general (Figure 5a). The results suggest that HPSC samples show better wear resistance compared to LPSC and GDC samples at every given load and temperature combination (Figure 5b). Such improved

tribological performance of the HPSC samples is attributed to the reduction in porosity and shrinkage defects. A higher wear rate is observed for the non-pressurized cast samples due to its high coefficient of friction, which is the result of poor surface quality along with the presence of porosities and shrinkage defects, whereas the coefficient of friction is less in pressurized cast samples, thereby increasing its tribological response. Samples fabricated by squeeze-casting process demonstrated lesser wear rate in comparison to GDC process. Squeeze pressure maintains the molten metal closer to the wall surfaces of the die, which in turn gives a higher cooling rate at the surface. Higher cooling rate results in a more refined dendritic structure, resulting in a smoother surface. Finer microstructures offer improved hardness, which in turn offer higher wear resistance [65–67]. It may be observed that in general, the wear resistance of the HPSC decreases with increasing load and/temperature combination due to accelerated conditions (which is as expected). Ashiri et al. [36] have shown similar wear properties on the Al–Si–Mg–Ni–Cu alloy fabricated by GDC and pressure squeeze cast samples. They have demonstrated that both wear rate and COF decrease with an increase in the pressure at a given load. The wear loss increases with an increase in the applied load. In addition, the COF of pressure squeeze-cast materials is lower than the GDC counterpart, and the results are in agreement with the present study.

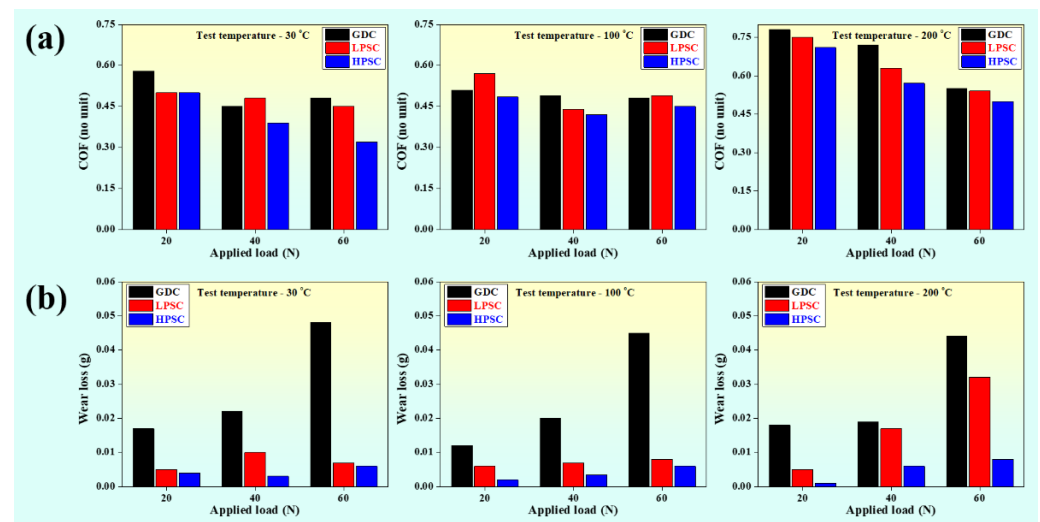


**Figure 5.** Tribological performance including (a) coefficient of friction and (b) wear loss comparison between GDC, LPSC, and HPSC samples as a function of load and operating temperature.

### 3.5. SEM Surface Analysis of the Worn out Samples

Fracture analysis conducted on worn-out samples by using SEM micrographs is shown in Figure 6. The wear surface of Al-based cast samples through the GDC route (Figure 6(a1,a2)) shows the presence of excessive material loss due to digging and penetration (deeper ploughing grooves [68,69]) of the pin at higher loads applied at elevated temperature. On the other hand, the LPSC samples wear surface shows minor digging and smearing observed due to frequent rubbing of the pin (Figure 6(b1,b2)). In addition, delamination and micro cracking (Figure 6(a1,a2)) may be observed in the samples produced through the GDC route due to its lower hardness compared to LPSC and HPSC samples. However, deep ploughing grooves and considerable delamination were not observed in the samples fabricated through LPSC and HPSC. The HPSC samples wear surface shows minimal rubbing/wear pattern at higher loads applied at elevated temperature. This difference in the wear rate of HPSC samples (Figure 6(c1,c2)) is due to the molten metal being solidified under high pressure, which reduces gas entrapments and shrinkages or gas porosity thereby improving its tribological properties, in addition to the microstructural refinement [70–72]. The present results are very similar to the studies conducted by Ashiri et al. [36], where deeper ploughing grooves are observed for the GDC samples compared with the pressure squeeze-cast samples leading to severe damage in the

GDC samples. Hence, the present results demonstrate the role of pressure during the casting/solidification process and its influence in refining the microstructure and improving their mechanical and tribological performance.

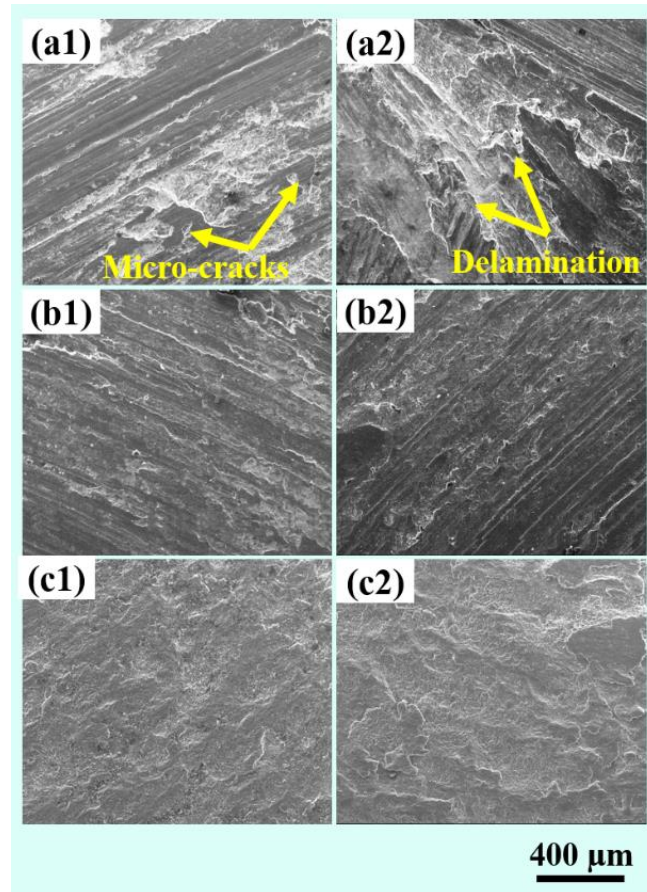


**Figure 6.** Worn out surface of the cast alloys in GDC, LPSC, an HPSC at two different load conditions 20 N (a1,b1,c1) and 60 N (a2,b2,c2) at a higher operating temperature of 200 °C.

#### 4. Conclusions

In this study, a varying cast pressure was applied to squeeze cast novel Al-Si alloys, and their effect on microstructure, mechanical properties, and wear behavior at higher operating temperatures were investigated and compared with GDC counterparts. The investigation reveals better mechanical behavior for squeeze cast Al-Si alloys compared to their GDC counterpart. In all cases, the HPSC alloy shows better mechanical behavior (hardness (115 HV) and tensile strength (540 MPa)) as compared to its GDC counterpart (hardness (86 HV), and tensile strength (367 MPa)). The microstructural study reveals reduced grain size, increased grain boundaries volume, reduction in dendrite arm spacing, small and rounded Si eutectic phases, and dendrites in the HPSC alloy. Wear behavior was studied at different loads 20 N and 60 N for the samples fabricated by GDC, LPSC, and HPSC routes. The results reveal the remarkable differences in wear rate, even at higher operating temperature and load for HPSC samples (wear loss 0.09 g), compared to the GDC (wear loss 0.045 g) and LPSC samples (wear loss 0.033 g) under nominal pressure due to minimal casting defects and lesser coefficient of friction. Under the same test condition, the HPSC samples show the least COF of 0.481 as against the GDC (COF—0.534) and LPSC (COF—0.516) samples. This study helps in determining the high-temperature wear-resistant behavior of a novel Al-Si HPSC alloy, making it suitable for critical industrial applications.

**Author Contributions:** V.S.C. has conducted the literature survey, development, testing and validation of the alloy. K.S.V.B.R.K. helped supporting in literature survey and manuscript draft preparation. M.R. supported in developing the alloy. K.S. contributed in conceptualization, methodology, critical analysis of data, reviewing and editing the manuscript. S.D. supported in formal analysis, data curation and resource allocation. K.G.P. supported in resources, review and editing the manuscript. All authors have read and agreed to the published version of the manuscript.

**Funding:** This research received no external funding.

**Institutional Review Board Statement:** Not applicable.

**Informed Consent Statement:** Not applicable.

**Data Availability Statement:** The results are a part of an ongoing study and the data will be made available on reasonable requests.

**Acknowledgments:** The authors would like to acknowledge the support rendered by Ramya Gopalakrishnan and Divya Sekar of M/s Ashok Leyland Ltd.—MED during testing of the samples.

**Conflicts of Interest:** The authors declare no conflict of interest.

## References

1. Brooker, A.D.; Ward, J.; Wang, L. Lightweighting impacts on fuel economy, cost, and component losses. *SAE Tech. Pap.* **2013**, *2*. [[CrossRef](#)]
2. Cann, J.L.; De Luca, A.; Dunand, D.C.; Dye, D.; Miracle, D.B.; Oh, H.S.; Olivetti, E.A.; Pollock, T.M.; Poole, W.J.; Yang, R.; et al. Sustainability through alloy design: Challenges and opportunities. *Prog. Mater. Sci.* **2021**, *117*, 100722. [[CrossRef](#)]
3. Imran, M.; Khan, A.R.A. Characterization of Al-7075 metal matrix composites: A review. *J. Mater. Res. Technol.* **2019**, *8*, 3347–3356. [[CrossRef](#)]
4. Vashisht, S.; Rakshit, D. Recent advances and sustainable solutions in automobile air conditioning systems. *J. Clean. Prod.* **2021**, *329*, 129754. [[CrossRef](#)]
5. Milman, Y.V. High-Strength Aluminum Alloys. *Met. Mater. High Struct. Effic.* **2004**, 139–150. [[CrossRef](#)]
6. Inoue, A. Amorphous, nanoquasicrystalline and nanocrystalline alloys in Al-based systems. *Prog. Mater. Sci.* **1998**, *43*, 365–520. [[CrossRef](#)]
7. Lin, T.C.; Cao, C.; Sokoluk, M.; Jiang, L.; Wang, X.; Schoenung, J.M.; Lavernia, E.J.; Li, X. Aluminum with dispersed nanoparticles by laser additive manufacturing. *Nat. Commun.* **2019**, *10*, 1–9. [[CrossRef](#)] [[PubMed](#)]
8. Wang, Z.; Ummethala, R.; Singh, N.; Tang, S.; Suryanarayana, C.; Eckert, J.; Prashanth, K.G. Selective laser melting of aluminum and its alloys. *Materials* **2020**, *13*, 4564. [[CrossRef](#)] [[PubMed](#)]
9. Sankaran, K.K.; Mishra, R.S. Aluminum Alloys. *Metall. Des. Alloy. Hierarchical Microstruct.* **2017**, 57–176. [[CrossRef](#)]
10. Kim, S.Y.; Lee, G.Y.; Park, G.H.; Kim, H.A.; Lee, A.Y.; Scudino, S.; Prashanth, K.G.; Kim, D.H.; Eckert, J.; Lee, M.H. High strength nanostructured Al-based alloys through optimized processing of rapidly quenched amorphous precursors. *Sci. Rep.* **2018**, *8*, 1–12. [[CrossRef](#)]
11. Gao, T.; Hu, K.; Wang, L.; Zhang, B.; Liu, X. Morphological evolution and strengthening behavior of  $\alpha$ -Al(Fe,Mn)Si in Al-6Si-2Fe-xMn alloys. *Results Phys.* **2017**, *7*, 1051–1054. [[CrossRef](#)]
12. Fabrizi, A.; Ferraro, S.; Timelli, G. The Influence of Fe, Mn and Cr Additions on the Formation of Iron-Rich Intermetallic Phases in an Al-Si Die-Casting Alloy. In *Shape Casting: 5th International Symposium 2014*; Wiley: Hoboken, NJ, USA, 2014; pp. 277–284. [[CrossRef](#)]
13. Wang, K.; Tang, P.; Huang, Y.; Zhao, Y.; Li, W.; Tian, J. Characterization of microstructures and tensile properties of recycled Al-Si-Cu-Fe-Mn alloys with individual and combined addition of titanium and cerium. *Scanning* **2018**, *2018*, 1–14. [[CrossRef](#)]
14. Prashanth, K.G.; Scudino, S.; Klauss, H.J.; Surreddi, K.B.; Löber, L.; Wang, Z.; Chaubey, A.K.; Kühn, U.; Eckert, J. Microstructure and mechanical properties of Al-12Si produced by selective laser melting: Effect of heat treatment. *Mater. Sci. Eng. A* **2014**, *590*, 153–160. [[CrossRef](#)]
15. Ma, P.; Jia, Y.; Prashanth, K.G.; Yu, Z.; Li, C.; Zhao, J.; Yang, S.; Huang, L. Effect of Si content on the microstructure and properties of Al-Si alloys fabricated using hot extrusion. *J. Mater. Res.* **2017**, *32*, 2210–2217. [[CrossRef](#)]
16. Ma, P.; Prashanth, K.; Scudino, S.; Jia, Y.; Wang, H.; Zou, C.; Wei, Z.; Eckert, J. Influence of Annealing on Mechanical Properties of Al-20Si Processed by Selective Laser Melting. *Metals* **2014**, *4*, 28–36. [[CrossRef](#)]
17. Prashanth, K.G.; Damodaram, R.; Scudino, S.; Wang, Z.; Prasad Rao, K.; Eckert, J. Friction welding of Al-12Si parts produced by selective laser melting. *Mater. Des.* **2014**, *57*, 632–637. [[CrossRef](#)]
18. Gokuldoss Prashanth, K.; Scudino, S.; Eckert, J. Tensile Properties of Al-12Si Fabricated via Selective Laser Melting (SLM) at Different Temperatures. *Technologies* **2016**, *4*, 38. [[CrossRef](#)]
19. Prashanth, K.G.; Scudino, S.; Chaubey, A.K.; Löber, L.; Wang, P.; Attar, H.; Schimansky, F.P.; Pyczak, F.; Eckert, J. Processing of Al-12Si-TNM composites by selective laser melting and evaluation of compressive and wear properties. *J. Mater. Res.* **2016**, *31*, 55–65. [[CrossRef](#)]

20. Zeren, M.; Karakulak, E.; Gümüş, S. Influence of Cu addition on microstructure and hardness of near-eutectic Al-Si-xCu-alloys. *Trans. Nonferrous Met. Soc. China* **2011**, *21*, 1698–1702. [[CrossRef](#)]
21. Ahn, S.S.; Pathan, S.; Koo, J.M.; Baeg, C.H.; Jeong, C.U.; Son, H.T.; Kim, Y.H.; Lee, K.H.; Hong, S.J. Enhancement of the Mechanical Properties in Al-Si-Cu-Fe-Mg Alloys with Various Processing Parameters. *Materials* **2018**, *11*, 2150. [[CrossRef](#)]
22. Basak, C.B.; Babu, N.H. Influence of Cu on modifying the beta phase and enhancing the mechanical properties of recycled Al-Si-Fe cast alloys. *Sci. Rep.* **2017**, *7*, 1–10. [[CrossRef](#)]
23. Taylor, J.A. Iron-Containing Intermetallic Phases in Al-Si Based Casting Alloys. *Procedia Mater. Sci.* **2012**, *1*, 19–33. [[CrossRef](#)]
24. Mathew, J.; Remy, G.; Williams, M.A.; Tang, F.; Srirangam, P. Effect of Fe Intermetallics on Microstructure and Properties of Al-7Si Alloys. *JOM* **2019**, *71*, 4362–4369. [[CrossRef](#)]
25. Taylor, A.J. The effect of iron in Al-Si casting alloys. In Proceedings of the 35th Australian Foundry Institute National Conference, Adelaide, Australia, 31 October–3 November 2004; pp. 148–157.
26. Górny, M. Fluidity and Temperature Profile of Ductile Iron in Thin Sections. *J. Iron Steel Res. Int.* **2012**, *19*, 52–59. [[CrossRef](#)]
27. Prashanth, K.; Scudino, S.; Chatterjee, R.; Salman, O.; Eckert, J. Additive Manufacturing: Reproducibility of Metallic Parts. *Technologies* **2017**, *5*, 8. [[CrossRef](#)]
28. Prashanth, K.G.; Scudino, S.; Eckert, J. Defining the tensile properties of Al-12Si parts produced by selective laser melting. *Acta Mater.* **2017**, *126*, 25–35. [[CrossRef](#)]
29. Rathod, H.J.; Nagaraju, T.; Prashanth, K.G.; Ramamurty, U. Tribological properties of selective laser melted Al-12Si alloy. *Tribol. Int.* **2019**, *137*, 94–101. [[CrossRef](#)]
30. Santosh, M.V.; Suresh, K.R.; Kiran Aithal, S. Mechanical Characterization and Microstructure analysis of Al C355.0 by Sand Casting, Die Casting and Centrifugal Casting Techniques. *Mater. Today Proc.* **2017**, *4*, 10987–10993. [[CrossRef](#)]
31. Srivastava, N.; Anas, M. An investigative review of squeeze casting: Processing effects & impact on properties. *Mater. Today Proc.* **2020**, *26*, 1914–1920. [[CrossRef](#)]
32. Kwok, T.W.J.; Zhai, W.; Peh, W.Y.; Gupta, M.; Fu, M.W.; Chua, B.W. Squeeze Casting for the Production of Metallic Parts and Structures. *Encycl. Mater. Met. Alloy.* **2022**, 87–99. [[CrossRef](#)]
33. Venkatesan, S.; Xavier, M.A. Analysis of Mechanical Properties of Aluminum Alloy Metal Matrix Composite by Squeeze Casting—A Review. *Mater. Today Proc.* **2018**, *5*, 11175–11184. [[CrossRef](#)]
34. Weiler, J.P. A review of magnesium die-castings for closure applications. *J. Magnes. Alloy.* **2019**, *7*, 297–304. [[CrossRef](#)]
35. Lus, H.M.; Ozer, G.; Guler, K.A. In Situ Composite of (Mg<sub>2</sub>Si)/Al Fabricated by Squeeze Casting. *TMS Annu. Meet.* **2012**, *1*, 775–781. [[CrossRef](#)]
36. Ashiri, R.; Niroumand, B.; Karimzadeh, F. Physical, mechanical and dry sliding wear properties of an Al-Si-Mg-Ni-Cu alloy under different processing conditions. *J. Alloys Compd.* **2014**, *582*, 213–222. [[CrossRef](#)]
37. Raji, A.; Khan, R.H. Effects of pouring temperature and squeeze pressure on the properties of Al-8%Si alloy squeeze cast components. In *Proceedings of the Institute of Cast Metals Engineers—67th World Foundry Congress, wfc06: Casting the Future*; Curran Associates Inc.: Red Hook, NY, USA, 2006; Volume 2, pp. 834–843.
38. Lin, B.; Zhang, W.W.; Lou, Z.H.; Zhang, D.T.; Li, Y.Y. Comparative study on microstructures and mechanical properties of the heat-treated Al-5.0Cu-0.6Mn-xFe alloys prepared by gravity die casting and squeeze casting. *Mater. Des.* **2014**, *59*, 10–18. [[CrossRef](#)]
39. Thirumal Azhagan, M.; Mohan, B.; Rajadurai, A. Optimization of process parameters to enhance the hardness on squeeze cast aluminium alloy AA6061. *Int. J. Eng. Technol.* **2014**, *6*, 183–189.
40. Brayshaw, W.J.; Roy, M.J.; Sun, T.; Akrivos, V.; Sherry, A.H. Iterative mesh-based hardness mapping. *Sci. Technol. Weld. Join.* **2016**, *22*, 404–411. [[CrossRef](#)]
41. Pongen, R.; Birru, A.K.; Parthiban, P. Study of microstructure and mechanical properties of A713 aluminium alloy having an addition of grain refiners Al-3.5 Ti-1.5C and Al-3Cobalt. *Results Phys.* **2019**, *13*, 102105. [[CrossRef](#)]
42. Zong, Y.Y.; Chen, L.; Zhao, Z.G.; Shan, D.B. Flow Lines, Microstructure, and Mechanical Properties of Flow Control Formed 4032 Aluminum Alloy. *Mater. Manuf. Processes* **2014**, *29*, 466–471. [[CrossRef](#)]
43. Chen, Z.; Yan, K. Grain refinement of commercially pure aluminum with addition of Ti and Zr elements based on crystallography orientation. *Sci. Rep.* **2020**, *10*, 1–8. [[CrossRef](#)]
44. Nadendla, H.B.; Nowak, M.; Bolzoni, L. Grain Refiner for Al-Si Alloys. *Miner. Met. Mater. Ser.* **2016**, 1009–1012. [[CrossRef](#)]
45. Guan, R.G.; Tie, D. A Review on Grain Refinement of Aluminum Alloys: Progresses, Challenges and Prospects. *Acta Metall. Sin.* **2017**, *30*, 409–432. [[CrossRef](#)]
46. Xi, L.; Gu, D.; Guo, S.; Wang, R.; Ding, K.; Prashanth, K.G. *Grain Refinement in Laser Manufactured Al-Based Composites with TiB<sub>2</sub> Ceramic*; Elsevier: Amsterdam, The Netherlands, 2020; Volume 9, pp. 2611–2622.
47. Singh, A.; Basha, D.A.; Matsushita, Y.; Tsuchiya, K.; Lu, Z.; Nieh, T.G.; Mukai, T. Domain structure and lattice effects in a severely plastically deformed CoCrFeMnNi high entropy alloy. *J. Alloys Compd.* **2020**, *812*, 152028. [[CrossRef](#)]
48. Arzaghi, M.; Fundenberger, J.J.; Toth, L.S.; Arruffat, R.; Faure, L.; Beausir, B.; Sauvage, X. Microstructure, texture and mechanical properties of aluminum processed by high-pressure tube twisting. *Acta Mater.* **2012**, *60*, 4393–4408. [[CrossRef](#)]
49. Lavernia, E.J.; Han, B.Q.; Schoenung, J.M. Cryomilled nanostructured materials: Processing and properties. *Mater. Sci. Eng. A* **2008**, *493*, 207–214. [[CrossRef](#)]

50. Liu, X.; Ma, P.; Ji, Y.D.; Wei, Z.J.; Suo, C.J.; Ji, P.C.; Shi, X.R.; Yu, Z.S.; Prashanth, K.G. Solidification of Al-xCu alloy under high pressures. *J. Mater. Res. Technol.* **2020**, *9*, 2983–2991. [[CrossRef](#)]
51. Ma, P.; Wei, Z.J.; Jia, Y.D.; Yu, Z.S.; Prashanth, K.G.; Yang, S.L.; Li, C.G.; Huang, L.X.; Eckert, J. Mechanism of formation of fibrous eutectic Si and thermal conductivity of SiCp/Al-20Si composites solidified under high pressure. *J. Alloys Compd.* **2017**, *709*, 329–336. [[CrossRef](#)]
52. Bayoumy, D.; Schliephake, D.; Dietrich, S.; Wu, X.H.; Zhu, Y.M.; Huang, A.J. Intensive processing optimization for achieving strong and ductile Al-Mn-Mg-Sc-Zr alloy produced by selective laser melting. *Mater. Des.* **2021**, *198*, 109317. [[CrossRef](#)]
53. Yap, C.Y.; Chua, C.K.; Dong, Z.L.; Liu, Z.H.; Zhang, D.Q.; Loh, L.E.; Sing, S.L. Review of selective laser melting: Materials and applications. *Appl. Phys. Rev.* **2015**, *2*, 041101. [[CrossRef](#)]
54. ASTM E8/E8M-16. *Standard Test Methods for Tension Testing of Metallic Materials*; ASTM International: West Conshohocken, PA, USA, 2016.
55. ASTM G99-05. *Standard Test Method for Wear Testing with a Pin-on-Disk Apparatus*; ASTM International: West Conshohocken, PA, USA, 2014.
56. Khan, S.; Ahmad, Z. Comparative analysis for coefficient of friction of LM 25 alloy and LM 25 granite composite at different sliding speeds and applied pressure. *Int. J. Mech. Prod. Eng. Res. Dev.* **2018**, *8*, 291–300. [[CrossRef](#)]
57. Feyzullahoğlu, E.; Şakiroğlu, N. The tribological behaviours of aluminium-based materials under dry sliding. *Ind. Lubr. Tribol.* **2011**, *63*, 350–358. [[CrossRef](#)]
58. Shanmugasundaram, P. Investigation on the Wear Behaviour of Eutectic Al-Si Alloy-Al<sub>2</sub>O<sub>3</sub>—Graphite Composites Fabricated Through Squeeze Casting. *Mater. Res.* **2014**, *17*, 940–946. [[CrossRef](#)]
59. Amar, M.B.; Souissi, S.; Souissi, N.; Bradai, C. Pressure and die temperature effects on microstructure and mechanical properties of squeeze casting 2017A wrought Al alloy. *Int. J. Microstruct. Mater. Prop.* **2012**, *7*, 491–501. [[CrossRef](#)]
60. Wei, Z.; Ma, P.; Wang, H.; Zou, C.; Scudino, S.; Song, K.; Prashanth, K.G.; Jiang, W.; Eckert, J. The thermal expansion behaviour of SiCp/Al-20Si composites solidified under high pressures. *Mater. Des.* **2015**, *65*, 387–394. [[CrossRef](#)]
61. Ma, P.; Zou, C.M.; Wang, H.W.; Scudino, S.; Fu, B.G.; Wei, Z.J.; Kühn, U.; Eckert, J. Effects of high pressure and SiC content on microstructure and precipitation kinetics of Al-20Si alloy. *J. Alloys Compd.* **2014**, *586*, 639–644. [[CrossRef](#)]
62. Maity, T.; Prashanth, K.G.; Balci, Ö.; Kim, J.T.; Schöberl, T.; Wang, Z.; Eckert, J. Influence of severe straining and strain rate on the evolution of dislocation structures during micro-/nanoindentation in high entropy lamellar eutectics. *Int. J. Plast.* **2018**, *109*, 121–136. [[CrossRef](#)]
63. Maity, T.; Prashanth, K.G.; Balçi, Ö.; Wang, Z.; Jia, Y.D.; Eckert, J. Plastic deformation mechanisms in severely strained eutectic high entropy composites explained via strain rate sensitivity and activation volume. *Compos. Part B Eng.* **2018**, *150*, 7–13. [[CrossRef](#)]
64. Maity, T.; Balci, Ö.; Gammer, C.; Ivanov, E.; Eckert, J.; Prashanth, K.G. High pressure torsion induced lowering of Young's modulus in high strength TNZT alloy for bio-implant applications. *J. Mech. Behav. Biomed. Mater.* **2020**, *108*, 103839. [[CrossRef](#)] [[PubMed](#)]
65. Chaubey, A.; Konda Gokuldoss, P.; Wang, Z.; Scudino, S.; Mukhopadhyay, N.; Eckert, J. Effect of Particle Size on Microstructure and Mechanical Properties of Al-Based Composite Reinforced with 10 Vol.% Mechanically Alloyed Mg-7.4%Al Particles. *Technologies* **2016**, *4*, 37. [[CrossRef](#)]
66. Mu, Y.; Zhang, L.; Xu, L.; Prashanth, K.; Zhang, N.; Ma, X.; Jia, Y.; Xu, Y.; Jia, Y.; Wang, G. Frictional wear and corrosion behavior of AlCoCrFeNi high-entropy alloy coatings synthesized by atmospheric plasma spraying. *Entropy* **2020**, *22*, 740. [[CrossRef](#)]
67. Wang, Z.; Georgarakis, K.; Zhang, W.W.; Prashanth, K.G.; Eckert, J.; Scudino, S. Reciprocating sliding wear behavior of high-strength nanocrystalline Al<sub>84</sub>Ni<sub>7</sub>Gd<sub>6</sub>Co<sub>3</sub> alloys. *Wear* **2017**, *382–383*, 78–84. [[CrossRef](#)]
68. Attar, H.; Prashanth, K.G.; Chaubey, A.K.; Calin, M.; Zhang, L.C.; Scudino, S.; Eckert, J. Comparison of wear properties of commercially pure titanium prepared by selective laser melting and casting processes. *Mater. Lett.* **2015**, *142*, 38–41. [[CrossRef](#)]
69. Ehtemam-Haghighi, S.; Prashanth, K.G.; Attar, H.; Chaubey, A.K.; Cao, G.H.; Zhang, L.C. Evaluation of mechanical and wear properties of Ti-xNb-7Fe alloys designed for biomedical applications. *Mater. Des.* **2016**, *111*, 592–599. [[CrossRef](#)]
70. Ma, P.; Wei, Z.J.; Jia, Y.D.; Zou, C.M.; Scudino, S.; Prashanth, K.G.; Yu, Z.S.; Yang, S.L.; Li, C.G.; Eckert, J. Effect of high pressure solidification on tensile properties and strengthening mechanisms of Al-20Si. *J. Alloys Compd.* **2016**, *688*, 88–93. [[CrossRef](#)]
71. Luo, D.; Zhou, Q.; Ye, W.; Ren, Y.; Greiner, C.; He, Y.; Wang, H. Design and Characterization of Self-Lubricating Refractory High Entropy Alloy-Based Multilayered Films. *ACS Appl. Mater. Interfaces* **2021**, *13*, 55712–55725. [[CrossRef](#)]
72. Hua, D.; Xia, Q.; Wang, W.; Zhou, Q.; Li, S.; Qian, D.; Shi, J.; Wang, H. Atomistic insights into the deformation mechanism of a CoCrNi medium entropy alloy under nanoindentation. *Int. J. Plast.* **2021**, *142*, 102997. [[CrossRef](#)]